Journal of Pharmaceutical Sciences 000 (2023) 1–11

Contents lists available at ScienceDirect

Journal of Pharmaceutical Sciences

journal homepage: www.jpharmsci.org

Pharmaceutics, Drug Delivery and Pharmaceutical Technology

Shifting the Focus from Dissolution to Permeation: Introducing the Meso-fluidic Chip for Permeability Assessment (MCPA)

Martina M. Tzanova[a], Bjarke Strøm Larsen[a], Rebecca Birolo[b], Sara Cignolini[c], Ingunn Tho[a], Michele R. Chierotti[b], Beatrice Perissutti[c], Silvia Scaglione[d], Paul C. Stein[e], Marianne Hiorth[a], Massimiliano Pio Di Cagno[a,*]

[a] Department of Pharmacy, Faculty of Mathematics and Natural Sciences, University of Oslo, Sem Saelands vei 3, 0371 Oslo, Norway
[b] Department of Chemistry and NIS centre, University of Torino, Via P. Giuria 7, 10125 Torino, Italy
[c] Department of Chemical and Pharmaceutical Sciences, University of Trieste, Via Alfonso Valerio, 6/1, 34127 Trieste, Italy
[d] National Research Council (CNR) and React4life S.p.A., Genoa, Italy
[e] Department of Physics, Chemistry and Pharmacy, University of Southern Denmark, 5230 Odense, Denmark

ARTICLE INFO

Article history:
Received 8 September 2023
Revised 12 December 2023
Accepted 12 December 2023
Available online xxx

Keywords:
Permeability
Dissolution/permeation
Amorphous solid dispersions
Crystalline adducts
MIVO®
Fluidics
PermeaPad®

ABSTRACT

In response to the growing ethical and environmental concerns associated with animal testing, numerous *in vitro* tools of varying complexity and biorelevance have been developed and adopted in pharmaceutical research and development. In this work, we present one of these tools, *i.e.*, the Meso-fluidic Chip for Permeability Assessment (MCPA), for the first time. The MCPA combines an artificial barrier (PermeaPad®) with an organ-on-chip device (MIVO®) and real-time automated concentration measurements, to yield a sustainable, yet effortless method for permeation testing. The system offers three major physiological aspects, *i.e.*, a biomimetic membrane, an optimal membrane interfacial area-to-donor-volume-ratio (A/V) and a physiological flow on the acceptor/basolateral side, which makes the MPCA an ideal candidate for mechanistic studies and excellent *in vivo* bioavailability predictions. We validated the method with a handful of assorted drug compounds in unstirred and stirred donor conditions, before exploring its applicability as a tool for dissolution/permeation testing on a BCS class III/I drug (pyrazinamide) crystalline adducts and BCS class II/IV (hydrocortisone) amorphous solid dispersions. The results were highly reproducible and clearly displayed the method's potential for evaluating the performance of enabling formulations, and possibly even predicting *in vivo* performance. We believe that, upon further development, the MCPA will serve as a useful *in vitro* tool that could push sustainability into pharmaceutics by refining, reducing and replacing animal testing in early-stage drug development.

Introduction

The growing recognition of both the ethical and environmental concerns surrounding animal testing has driven the pharmaceutical science community to explore strategies that can reduce, replace and refine these (the 3Rs principle [Russel & Burch, 1959]). Thus, *in vitro* permeation testing has become a pivotal and powerful tool, which allows researchers to gain, quickly and easily, an understanding of drug permeability across *in vivo* biological barriers. By assessing the ability of an active pharmaceutical ingredient (API) to cross various types of membranes, permeation testing provides valuable insights into the mechanisms governing drug absorption, and ultimately aids the decision-making process in the search for best candidates for drug and formulation development.

Numerous systems of varying levels of complexity and biological relevance have been developed and used for the experimental evaluation of drug permeability and formulation efficiency.[1,2] Regarding the type/source of permeation barrier intended for studying oral drug absorption, these can roughly be divided in the following groups: tissue-based,[3] cell-based[4] and cell-free,[5] with each of these providing different amount and type of information about drug permeation. Using excised animal or human tissue *ex vivo* preserves the gut architecture and some important physiological aspects (*e.g.*, the presence of enzymes and mucus) and allows the evaluation of multiple drug transport/absorption pathways, in addition to drug metabolism. Main disadvantage of these methods is the laborious preparation of delicate samples with large batch-to-batch variations

* Corresponding author.
E-mail address: m.p.d.cagno@farmasi.uio.no (M.P. Di Cagno).

https://doi.org/10.1016/j.xphs.2023.12.012

and poor experimental reproducibility, alongside some serious ethical and sustainability implications. Somewhat less laborious but in no way less time-consuming and expensive, are the techniques involving cell culturing. This usually takes place over multiple weeks and the experiments are a subject to large intra- and interlaboratory variation. The main advantage of cell-based permeation assays over cell-free ones is the possibility for evaluating active drug transport in and out of the cells.

A recent review by Jacobsen et al. [2023] focuses on the commercially available cell-free systems and the sustainability aspect, implying yet another beneficial aspect of these setups – their availability and ease of use. Biomimetic artificial membranes are namely cost-effective; they allow rapid and reproducible high-throughput screening, without any of the safety and storage limitations of the other two types of membranes[6] and are much more robust than a cellular barrier, allowing also testing of enabling formulations.[7] Multiple set-up options are commercially available for such studies, both large (*e.g.*, vertical and side-by-side diffusion cells) and small (*e.g.*, multi-well plates) volume-scaled.

For formulation testing, in the last years there has been a growing interest in combined dissolution/permeation systems, going beyond the limitations of classical Pharmacopoeial dissolution methods. From a commercial perspective, the MacroFLUX™ and BioFLUX™ from Pion Inc. and the Dissoflux from Electrolab India Pvt Ltd can be considered as the state-of-the-art of dissolution and permeation. Both systems are based on standard dissolution vessels in which an insert equipped with a biomimetic barrier (PAMPA and/or PermeaPad®, respectively) is mounted. As output, these systems provide both a classical dissolution profile of the oral formulation (*i.e.*, analyzing the donor compartment) and the drug's permeation profile (*i.e.*, analyzing the donor compartment) [8,9; Electrolab]. Both systems involve rather expensive instrumentation and require a significant amount of formulation (grams scale) as well as dissolution media to operate (order of magnitude of 10^0–10^1 L of water, depending on the number of replicates). On a prototype level, the recently introduced PermeaLoop™[10] setup has significant technological advantages in comparison to the commercial dissolution/permeation systems available. First, it has an optimal membrane interfacial area-to-donor-volume-ratio (A/V, of 1.38 cm^{-1}) which is much closer to the *in vivo* situation[11] in comparison to available commercial systems (order of magnitude of 10^{-3} cm^{-1}). The PermeaLoop™ proved to be an efficient system with increased *in vitro-in vivo* correlation (IVIVC) of oral formulation of BCS class II compound such as linifanib[10] and posaconazole,[12] and, more recently, also itraconazole.[13] Despite its great potential and promising results, thus far PermeaLoop™ remains a niche system with limited implementations mainly due to its lack of commercial availability.

Hence, the aim of this work was to develop a sustainable meso-fluidic system for permeability assessment and formulation testing, possessing the following pillars:

1. Cost-effectiveness
2. Easy to implement and user-friendly
3. Minimal operator handwork
4. Rational design, matching relevant United Nations' Sustainable Development Goals (SDGs, *e.g.*, No. 6 Clean Water and Sanitation, No. 10 Reduced Inequalities, No. 13 Climate Action).

For this purpose, we assembled the meso-fluidic chip for permeation assessment (MCPA), utilizing the commercially available fluidic disposable cell-culture chamber, MIVO®, by React4Life (depicted in Fig. 1, later in the text). The MIVO® was originally designed and developed as an organ-on-a-chip for tissue engineering studies on samples of clinically relevant sizes under dynamic conditions resembling the complex human physiology.[14,15] This novel and adaptable multipurpose technology has numerous applications in disease modelling, regenerative medicine and immunology. Furthermore, it offers a convenient *in vitro* platform for drug discovery, hereunder investigating drug efficacy, toxicity and pharmacokinetics.[1] So far, the MIVO® based platform has been reported to be a successful experimental approach for cell-[14] and tissue-based[16] permeation studies. The MIVO® was chosen for the purpose of this study due to its potentially optimal A/V ratio, and the possibility to equip it with the biomimetic barrier PermeaPad®, which is the most robust and biomimetic artificial barrier available[17] for permeation studies. To reduce to a minimum the effort for the operator, we automatized the system by connecting the acceptor loop of the system directly to a UV/Vis spectrophotometer with the use of flow-through cuvettes. To validate the MCPA, we investigated various drug solutions at different conditions, *i.e.*, concentrations and stirring rates.

Finally, we investigated the system's potential as a dissolution/permeation setup on co-crystals of the BCS class III/I[18] antitubercular

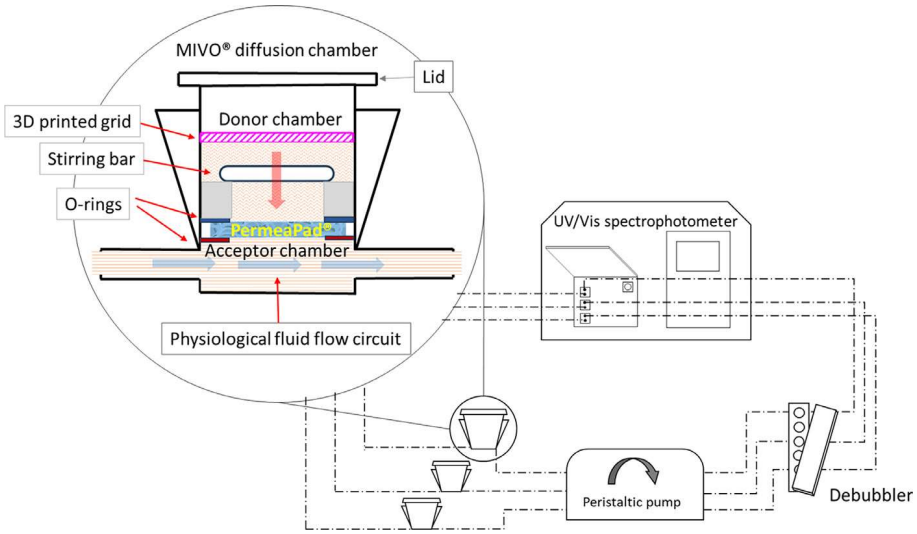

Figure 1. Schematic representation of the MCPA setup. Stippled lines (• – • – •) connecting the different components represent silicone tubing (Ø=2 mm).

drug, pyrazinamide, and simple polymer-based amorphous solid dispersions (ASDs) of the BCS class II/IV steroid drug, hydrocortisone. These formulations were chosen as examples of enabling strategies for improving drug bioavailability by altering its dissolution behaviour and/or solubility. Multicomponent crystalline adducts have been successfully applied to improve the physicochemical properties (*e.g.*, solubility, dissolution profile, permeability, pharmacokinetics and stability) of APIs without altering their intrinsic therapeutic action.[19] Despite the numerous case studies reported in the literature,[20–23] there is no commonly accepted theory regarding the modulations of drug permeability through co-crystallization.[24] On the other hand, amorphous drugs possess remarkable advantages with respect to solubility and dissolution rates compared to their crystalline counterparts but often suffer from poor stability leading to rapid re-crystallization. ASDs have been demonstrated to increase the *in vivo* bioavailability, possibly owing largely to the formation and stabilization of supersaturated solutions.[25,26]

Materials and Methods

Materials and Solvent Solutions

Atenolol (≥ 98 % TLC; ATN), caffeine (ReagentPlus®; CAF), ibuprofen (≥ 98 % GC; IBP), hydrocortisone (≥ 98 % HPLC; HC), ketoprofen (≥ 98 % TLC; KTP), paracetamol (PCT), 2,5-dihydroxyterephthalic acid (DHTA), maleic acid (MLEA), malic acid (MLIA), mandelic acid (MANDA) and sodium hydroxide (≥ 98.0% pellets; NaOH) were purchased from Sigma-Aldrich Chemie GmbH (Steinheim, DE). Potassium dihydrogen phosphate (KH_2PO_4), pyrazinamide (> 99 %; PZD), sodium dihydrogen phosphate dihydrate ($NaH_2PO_4{\cdot}2H_2O$), disodium phosphate dihydrate ($Na_2HPO_4{\cdot}2H_2O$), sodium chloride (NaCl), tert-butanol (≥ 99 % GC) were obtained from Merck KGaA (Darmstadt, DE), while dipicolinic acid (DPA) and trimesic acid (TRMA) were purchased from Alfa Aesar Chemicals (Ward Hill, MA, USA). Polyvinylpyrrolidone (Kollidon 12; PVP) was acquired from BASF Pharma (Ludwigshafen, DE) and (hydroxypropyl)methyl cellulose (Hypromellose 5; HPMC) was acquired from Norsk Medisinaldepot (NMD, Oslo, NO). All reagents were used as received. Phosphate-buffered saline (PBS; 73 mM) was prepared by dissolving 5 g/L $NaH_2PO_4{\cdot}2H_2O$ and 7.2 g/L $Na_2HPO_4{\cdot}2H_2O$ in Milli-Q® ultrapure water (Merck Millipore; Darmstadt, DE) and adjusting the pH to 7.4 ± 0.05 (SevenCompact™ pH/ion meter S220; Mettler Toledo, Columbus, OH, USA) with NaOH and the osmolality to 280–300 mOsm/kg (Semi-Micro Osmometer K-7400, Knauer, Berlin, DE) with NaCl. The solution was filtered 0.2 μm (Whatman® Nuclepore Track-Etch membrane filter; GE Healthcare Life Sciences, Maidstone, UK) prior to use.

Drug Diffusivity

The diffusion coefficients of all investigated compounds were determined with the UV/Vis localized spectroscopy previously presented (Tzanova et al. [2021]). A 1 mM solution of each drug in PBS was prepared and 25 μL were injected with the help of a microneedle syringe (Hamilton Company, Reno, NV, USA) on the bottom of a semi-micro cuvette with PTFE stopper (light path = 10 mm; $V_{chamber}$ = 700 μL, Starna Scientific®, Essex, UK) filled with 675 μL ultrapure water (*i.e.*, diffusion medium). The measurements were blank-corrected and performed on double array UV/Vis spectrophotometer UV-6300PC over a total period of at least 21 hours with absorbance recording every 120 seconds. The respective λ_{max} for each drug was used for the measurements (Table 1). The diffusion profiles obtained by these measurements were fitted to the analytical solution of the Fick's second law of diffusion presented by Di Cagno et al. [2018] together with the initial report on the method, Eq. (1):

$$c(x,\ t) = \frac{2A}{\sqrt{\pi}} \frac{e^{\frac{-x^2}{2\sigma^2+4Dt}}}{\sqrt{2\sigma^2+4Dt}} \quad (1)$$

Where t is time (s) of the measurement and c is the concentration (mM) at that given time point, x is the distance between origin of diffusion and detection point (= 0.51 cm); D (cm^2/s), A ($mmol/cm^2$) and σ (cm) are fitting parameters representing the drug diffusivity, initial drug fraction and the width of the initial drug distribution, respectively.

Preparation of Donor Samples

In order to establish and validate the new setup and methodology, the permeability of seven different APIs was measured: atenolol, caffeine, hydrocortisone, ibuprofen, ketoprofen, paracetamol and pyrazinamide. Initially, solutions of caffeine, ibuprofen and ketoprofen were prepared at different concentrations (0.5, 1, 2, 2.8 and 5 mM) with the aim of determining the optimal concentration for future experiments. Further, 2 mM solutions of each drug in PBS were used as the standard donor solution (C_0), with hydrocortisone being too poorly soluble and used as a saturated solution instead (*i.e.*, $C_0 = C_{sat}$). An overview of all tested solutions, as well as a summary of the physico-chemical characteristics of all compounds can be found in Table 1. For testing the formulations (see Sections 2.4 and 2.5), dry samples were weighed and added to the donor chamber, together with a magnetic stir bar and a 3D-printed plastic grid, designed to ensure undissolved particles remained in contact with the bulk solvent instead of floating to the top (design details provided in Appendix A, Fig. A1). The amount of pyrazinamide formulations (Section 2.4) added corresponded to 2 mM final concentration, whilst the hydrocortisone formulations (Section 2.5) were added in an amount resulting in five times the thermodynamic solubility. Finally, 2 mL of PBS pH 7.4 were added to the donor chamber.

Preparation and Characterization of Pyrazinamide Crystalline Adducts

Crystalline adducts of pyrazinamide and one of six acidic coformers were prepared by slurry technique or liquid-assisted grinding (LAG). Briefly, for the slurry synthesis, the powders of the two reactants were added to a 10 mL beaker with 1 mL solvent. The sample was left under agitation for two days at ambient conditions. The LAG procedure was performed in a mortar and involved milling the starting materials with a pestle and adding three drops of solvent every 10 minutes for a total of 30 minutes. The detailed experimental conditions, including the solvent, the stoichiometric ratio and the amounts of reagents used are provided in Table 2.

Dried powder samples were analysed by Fourier-transform infrared with attenuated total reflection (FTIR-ATR) and powder X-ray diffraction (PXRD) to confirm the formation of a new crystal form. FTIR-ATR spectra were collected on an Equinox 55 (Bruker Scientific Instruments; Billerica, MA, USA) in the 400-4000 cm^{-1} range with a resolution of 2 cm^{-1} and 16 scans. X-ray powder patterns of samples obtained by slurry and LAG were recorded on an X'pert Pro (45 kV, 40000 μA) diffractometer (PANalytical, Malver, UK) in the Bragg-Brentano geometry, using Cu–Kα radiation (λ = 1.5418 Å) in the 2θ range between 5° and 50° (continuous scan mode, step size 0.0167°, counting time 40 s).

Preparation and Characterization of Hydrocortisone Amorphous Solid Dispersions

Amorphous solid dispersions (ASDs) of hydrocortisone with either PVP or HPMC were prepared by freeze-drying solutions of drug and polymer in an Alpha 2-4 LDplus benchtop freeze-dryer (Martin Christ Gefriertrocknungsanlagen GmbH; Osterode, DE) equipped with an external RV5 vacuum pump (Edwards Vacuum; Burgess Hill, UK).

Table 1
Summary of physico-chemical properties of atenolol (ATN), caffeine (CAF), ibuprofen (IBP), hydrocortisone (HC), ketoprofen (KTP), paracetamol (PCT) and pyrazinamide (PZD). Overview of measured aqueous diffusivities (D), the wavelength (λ_{max}) used for each compound, the donor concentration(s) (C_0) tested of each, the stirring conditions of the permeability experiments and the type of donor samples tested.

Compound/API	M_w (g/mol)	pK_a*	logP*	λ_{max} (nm)	D ($\times 10^{-6}$ cm^2/s)	C_0 (mM)	Stirring (with/without)	Donor samples
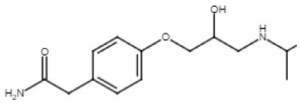 ATN	266.3	9.58	0.16	225	4.34	2.0	Both	Solution
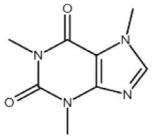 CAF	194.2	14.00	-0.07	273	7.06	0.5** 1.0** 2.0 2.8** 5.0**	Both (at speed settings 2-10, *i.e.* 250-1200 rpm)	Solutions
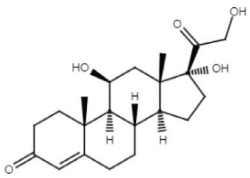 HC	362.5	12.6	1.61	248	4.45	0.8 5×C_{sat}	Both ASD: With	• Solution • PVP ASD • HPMC ASD
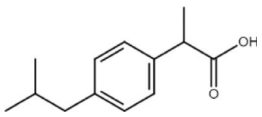 IBP	206.3	4.45	3.97	221	6.05	0.5** 1.0** 2.0 2.8** 5.0**	Both	Solutions
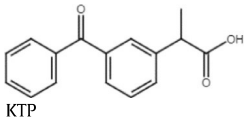 KTP	254.3	3.98	3.13	261	5.43	0.5** 1.0** 2.0 2.8** 5.0**	Both	Solution
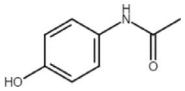 PCT	151.2	9.38	0.46	242	7.32	2.0	Both	Solution
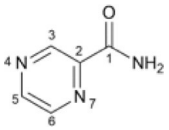 PZD	123.1	0.60	-0.60	269	9.14	2.0	Both Add.: With	• Solution • Crystalline adducts

* Source: PubChem.
** These experiments were performed only once (n = 1).

Solutions of 4.5 mg/mL hydrocortisone and 40 mg/mL PVP or HPMC in solvent mixtures made of 70 % (v/v) tert-butanol in ultrapure water were prepared by stirring overnight with a magnetic stirrer. Aliquots (1 mL) of the prepared solutions were added to each well in a 24-well plate (Corning Inc.; NY, NY, USA) with 1 mm holes drilled in the lid over each well and then rapidly frozen in a -80°C freezer for 2 hours before being placed in the freeze-dryer. The frozen samples were dried over 24 hours on an unheated shelf at a pressure of 0.011 mbar with the condenser at a temperature of -87°C. Freeze-dried cakes with PVP were porous and brittle, while HPMC-based cakes were porous and light. These freeze-dried cakes were then blended in an electric coffee mill (Bistro, Bodum Inc.; Triengen, CH) to create coarse powder and then stored in a desiccator over dry silica gel until further use. A calorimetric method was employed to confirm the amorphous state of hydrocortisone. Differential scanning calorimetry (DSC) was performed on a DSC 822e (Mettler Toledo GmbH; Greifensee, CH) equipped with a Haake EK90/MT external cooler (Thermo Fisher Scientific; Dreieich, DE). Samples of approximately 5 mg powder were weighed into 40 μL aluminum crucibles with punctured lids (Mettler Toledo GmbH; Greifensee, CH). Freeze-dried samples were gently compacted into the crucible after weighing using a small cylindrical steel rod to improve surface contact with the bottom of the crucible. To avoid heat flow signal related to water evaporation from the hygroscopic material, samples containing PVP or HPMC were *in-situ* dried in the DSC before measurement by being rapidly heated to 95°C and kept isothermal for 2 min before being cooled to 25°C. Subsequently, these samples were scanned by heating from 25°C to 250°C with a heating rate of 20°C/min. Samples of crystalline hydrocortisone were measured as received using the same scanning protocol without the drying step. Measurements and *in-situ* drying were done under a dry nitrogen gas flow of 80 mL/min.

Permeability Testing with the MCPA

The MCPA setup used in this work is sketched in Fig. 1. The setup consisted of three MIVO® diffusion chambers (React4Life S.p.A., Genoa, IT) connected in parallel, a debubbler, a multichannel peristaltic pump (ISMATEC ISM931C, Wertheim, DE) and a double array UV/Vis spectrophotometer UV-6300PC equipped with an 8-position cell holder with auto cell-changer and 10 mm flow-through cells (all:

Table 2
Summary of coformers involved in the preparation of pyrazinamide (PZD) crystalline adducts and properties crucial to the process. Amount of PZD used in each synthesis was 100 mg and the stoichiometry was 1:1. ΔpK_a^*/prediction, indicates predicted outcome of the crystalline adducts according to[27].

Coformer	pK_a	ΔpK_a^*/ Prediction	Amount of coformer (mg)	Synthesis technique	Solvent
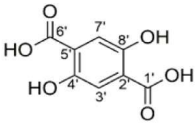 2,5-dihydroxyterephthalic acid (DHTA)	3.51	-2.91/ Cocrystal	161	LAG	acetone
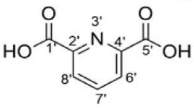 dipicolinic acid (DPA)	2.16	-1.56/ Cocrystal	136	Slurry	ethanol
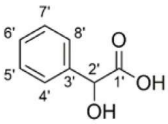 mandelic acid (MANDA)	3.41	-2.81/ Cocrystal	124	Slurry	ethylacetate
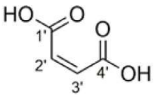 maleic acid (MLEA)	1.92	-1.32/ Cocrystal	94	Slurry	ethanol
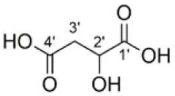 malic acid (MLIA)	3.40	-2.80/ Cocrystal	109	Slurry	ethanol
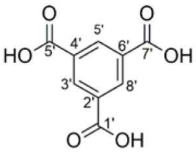 trimesic acid (TRMA)	3.12	-2.52/ Cocrystal	171	LAG	water

* Calculated as $\Delta pKa = pK_a$ (protonated PZD base) − pK_a (strongest coformer acid).

VWR International, Radnor, PA, USA), all connected by silicone tubing. The MIVO® chambers each hosted a 14 mm ready-to-use PermeaPad® biomimetic membrane (Phabioc GmbH, Karlsruhe, DE), sandwiched between two O-rings and held in place by an add-on (Fig. 1). The space within the chamber above the membrane was regarded as the donor compartment ($V_{donor} \leq 2$ mL), while the PBS flowing in a loop underneath the membrane was the acceptor compartment ($V_{acceptor} = 8$ mL, arbitrarily chosen). Each MIVO® chamber was placed in a 3D-printed holder, adapted to the magnetic stirrer used (see design in Appendix A) and was closed tightly with the accompanying lid. Acceptor medium was filled gradually through the debubbler to ensure no air bubbles remained trapped in the system. During the experiment, the flow rate was set to 2 mL/min, generating a velocity resembling the *in vivo* capillary blood flow.[14,16] The donor was either unstirred or stirred at speed 4 (≈ 500 rpm; IKA®-Werke GmbH & Co. RO 5 P, Staufen, DE) for all other samples except CAF, which was additionally investigated at speed 2, 6, 8 and 10 (≈ 250, 750, 1000 and 1200 rpm, respectively) for all solutions and always stirred when solid formulations were investigated. The spectrophotometer was set in "time scanning" mode and the absorbance data from each acceptor cuvette was collected every 120 seconds (arbitrary chosen) for a total of 3 hours, all absorbances blank-corrected by an additional reference cuvette filled with PBS. Drug concentrations in the acceptor at each time point were calculated using calibration curves ($R^2 \geq 0.999$; absorbance range: 0.05–1), and further converted to quantity (Q; μmol). In the case of drug solutions as donors, the cumulative quantity, Q, was normalized over the surface area of the membrane available for permeation (A = 0.43 cm^2) and plotted as a function of time. The drug flux (J; $\mu mol/cm^2 \times s$) was determined as the slope of the least squares linear regression between 3600 and 10,800 seconds (avoiding any potential lag time), and normalized over the starting donor concentration, C_0, to obtain the apparent permeability coefficient (P_{app}; cm/s), as summarized in Eq. (2).

$$P_{app} = \frac{J}{C_0} \tag{2}$$

Permeability Testing with PermeaPad® Multiwell Plate

In order to compare the results from the novel MCPA method, permeability testing with a previously established method [e.g.,[28,29]] method using PermeaPad® 96-well plate (Phabioc GmbH; Espelkamp, DE) was also performed. Four APIs from the drug pool were chosen for these experiments: atenolol, caffeine, hydrocortisone and

ketoprofen, and the same donor solutions described in Section 2.3 were used. Briefly, 200μL of each drug donor solution was applied to the top/insert plate, and 400μL PBS were applied to the bottom acceptor plate. The plate was incubated in an orbital shaker-incubator (ES-20, Biosan, Riga, LV) at 25 °C and rotation of 200 rpm for a total of 3 hours. Sampling from the acceptor took place every 30 minutes and the withdrawn volume (100 μL) was replenished by fresh PBS. The samples were analysed on a SpectraMax 190 microplate spectrophotometer (Molecular Devices Inc., Sunnyvale, CA, USA) in 96-well acrylic plates with UV-transparent flat bottom (Corning Inc., Kennebunk, ME, USA), alongside standard solutions (calibration curve $R^2 \geq 0.999$) and blank PBS samples. The cumulative amount of drug in the acceptor was used as Q in the aforementioned (Section 2.6) approach to obtaining P_{app}. The experiment was performed in triplicate.

Solubility of Pyrazinamide and Hydrocortisone

The thermodynamic solubility of pyrazinamide, all crystalline adducts and hydrocortisone was determined with the classical shake-flask method. Samples were prepared by adding excess of the respective compound in 5 mL PBS. The suspensions were kept at ambient temperature and stirred for 24 hours to achieve equilibrium between the solid and the dissolved phase. The suspensions were filtered (0.2 μm polyethersulfone (PES) syringe filter; VWR International, Radnor, PA, USA), and the filtrate was diluted adequately prior to spectrophotometric quantification of the dissolved drug. For hydrocortisone the same filtrate was used in the permeability testing.

Results and Discussion

The results and discussion are presented in increasing complexity, beginning with the establishment of method parameters and method validation using permeability profiling of seven different pharmaceutical compounds (atenolol, caffeine, hydrocortisone, ibuprofen, ketoprofen, paracetamol and pyrazinamide), and continuing with dissolution/permeation testing of pyrazinamide crystalline adducts and hydrocortisone ASDs.

Method Establishment and Validation

In the classical experimental setups for permeability testing, the manual handling of the sample to collect data points for creating the drug flux profile, Q/A vs time, not only introduces an additional source of experimental error but also limits the number of points and the time resolution of such analyses. Moreover, the initial part of the permeation curve, containing information about the lag time of the process preceding the steady-state permeation, can be lost in the classical experiments. Interestingly, this lag time contains information about the donor and acceptor aqueous unstirred water layers (UWL), and is strongly dependent on their influence on permeation.[29] In the MCPA, these issues are minimized by the large number of data points collected by the direct online analysis of the acceptor media throughout the entire experimental run, and by the efficient dynamic fluid flow conditions that can be achieved in both donor (with the stirring bar) and acceptor compartments (with the peristaltic pump). Fig. 2 exemplifies the data output obtained from the MCPA for caffeine in the absence (black triangles) and presence of stirring (speed 4, green circles) in the donor compartment, demonstrating the hight resolution of the measurements (i.e., every two minutes), the low standard deviation and the effect of stirring. As illustrated by Fig. 2, when stirring is not applied, the flux is pronouncedly lower than in stirred conditions. In fact, the steady-state flux measured (1–3 hours interval) was about 66 % higher for the stirred conditions than the unstirred conditions. Since the caffeine nominal concentration was the same in

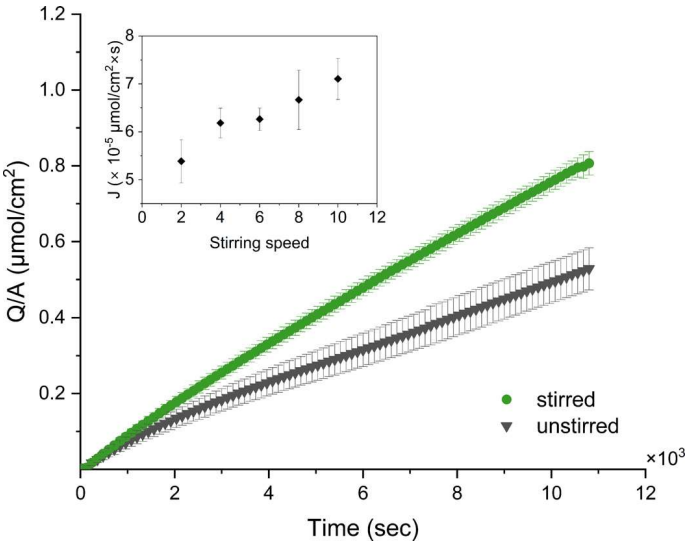

Figure 2. Caffeine (CAF) permeation curves in stirred (green circles) and unstirred (grey triangles) conditions in the on-line MCPA system. The plot illustrates a typical permeation curve in the system, expressed as the cumulative amount of drug permeated (Q) per membrane area (A) over time. Inset graph shows correlation (R^2 = 0.9412) between stirring speed and flux (J) for the same drug. Error bars show SD (n = 3).

the two experiments, this implies that the donor UWL is a major impediment to caffeine permeation, as previously demonstrated.[29] Additionally, the permeability of caffeine at different stirring rates in the speed range 2–10 (approx. 250–1200 rpm) was investigated. The results (Fig. 2, inset) showed almost linear increase over the entire speed range tested. This indicates that stirring in the donor compartment of the MCPA effectively reduces the UWL thickness. Thus, all further stirred experiments were performed at speed of 4, which produces a sufficient reduction in UWL effect. The next step in the development of MCPA was to determine the influence of drug concentration on the empirical permeability measured. Thus, caffeine and ketoprofen were chosen as a highly and moderately permeable compound, respectively, whilst ibuprofen was chosen for its low λ_{max}, *i.e.*, most prone to detector variability. The permeability of these compounds was tested without donor stirring at five different concentrations. For ibuprofen, each experiment was additionally performed in stirred conditions. No light scattering or unexpected absorbance deviating from linear steady-state-flux was observed for ibuprofen (both in static and stirred donor conditions). In the case of caffeine and ketoprofen, it appeared that a variation of the donor concentration had a minor effect on the net apparent drug permeability (Fig. 3). On the other hand, for ibuprofen, the drug donor concentration played an appreciable role on the calculated apparent permeability coefficient, P_{app}, under both investigated conditions, indicating that this phenomenon is an inherent property of the molecule and not necessarily dependent on the conditions of the system. These concentration-dependent discrepancies in the widely accepted parameter for comparing drug permeability, P_{app}, are something to be aware of as they can have a great impact on results interpretation. For the particular case of ibuprofen and other propionic acid derivatives, it is known that they have a tendency to form dimers.[30,31] The formation of dimers increases the hydrodynamic radius of the permeant, reducing its net flux through the barrier. This, in turn, can explain the lower observed permeability of ibuprofen at higher drug concentrations. In order to minimize the concentration effect, we decided to utilize drug concentrations of 2 mM and lower for further studies.

The results from the permeability profiling of all drugs under the established conditions are presented in the inset tables in Fig. 4 (in unstirred and stirred conditions in a) and b), respectively). All

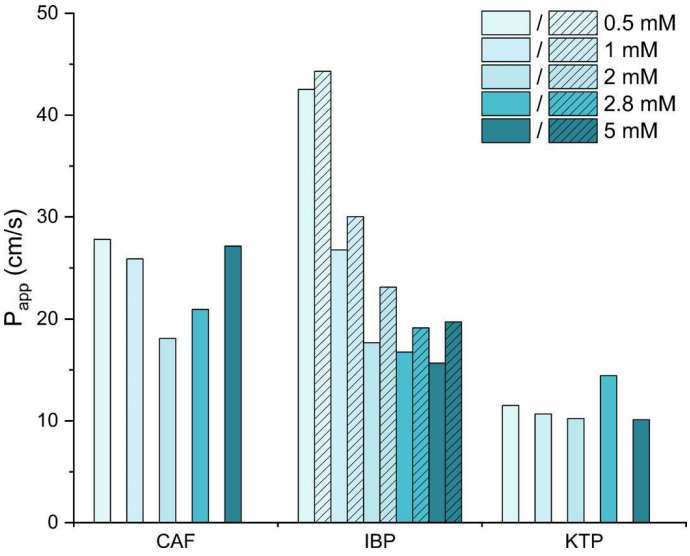

Figure 3. Caffeine (CAF), ibuprofen (IBP) and ketoprofen (KTP) apparent permeability coefficients (P_{app}) in the on-line MIVO®-PermeaPad® setup when different donor concentrations (C_0) were used. Colours indicate the concentration; *clean* columns show results in unstirred donor condition, while *patterned* columns (for IBP) show results in stirred condition.

compounds exhibited higher permeability from stirred donor conditions, although some were more strongly affected than others. As mentioned earlier, caffeine is an example of a compound with UWL-limited permeation. On the other hand, atenolol, a BCS class III compound with low permeability,[32] shows a marginal difference within stirred and unstirred conditions. Due to the novelty of the system, a comparison to well-established and earlier documented methods was necessary. For this reason, we correlated the P_{app} of atenolol, caffeine, hydrocortisone and ketoprofen measured in the MCPA to the P_{app} obtained by the standard PermeaPad® 96-well plate setup. The permeability results obtained with PermeaPad® plate and the MCPA are in the same order of magnitude and comprised within 10^{-6} and 10^{-5} cm/sec. Moreover, the correlation within P_{app} is overall acceptable, as demonstrated in Fig. 4, thus confirming the adequacy and usability of the novel method presented in this work. The P_{app} of hydrocortisone seems to be underestimated by the plate method and the removal of this point improves the linear correlation coefficient, R, from 0.89 to 0.99 and from 0.92 to 0.99 for unstirred and stirred conditions, respectively. This discrepancy is most likely owed to insufficient stirring provided by the classical orbital shaker, as discussed by Eriksen et al.,[33] which nevertheless remains the standard stirring method for multiwell *in vitro* permeation assays. The hydrocortisone results from the MCPA are anyway in the same order of magnitude with other methods[17,34] and even results from the PermeaPad® plate when magnetic stirring in the donor is used.[35] A recent work by Pulsoni et al. [2022] concluded that the MIVO® system better predicts the transdermal permeability of lipophilic compounds in line with *in vivo* data, owing to the physiological flow underneath the investigated permeation barriers.

The trend in P_{app} measured with the MCPA agrees with the results obtained with other classical permeation assays, with some discrepancies. For atenolol and ketoprofen, a work by Teksin et al.[36] provides a comparison to the PAMPA system in unstirred conditions. Ketoprofen shows a remarkable similarity between the two systems (12.6 ± 0.5 cm/s for PAMPA vs 10.2 ± 1.3 cm/s for MPCA-unstirred conditions vs 15.4 ± 1.8 cm/s for MPCA-stirred conditions). Interestingly, for hydrocortisone and caffeine, whose permeations are notably affected by the UWL, the P_{app} measured with a classic non-fluidic PAMPA system[37] result for 2 to 4.5 lower than with the MPCA, further demonstrating the role played by a fluidic acceptor environment. The P_{app} for atenolol, caffeine and hydrocortisone obtained through the MCPA are well in agreement also with Caco-2 permeability data,[34] suggesting better predictivity of this model, compared to others. Jacobsen et al. [2020] have worked with caffeine and hydrocortisone, and the same permeation membrane in a 96-well plate format, using magnetic stirring in the acceptor compartment, and report values close to the ones reported here.

Pyrazinamide Crystalline Adducts

The MCPA was further developed to test solid dosage formulations. For this purpose, a series of multicomponent crystalline adducts of pyrazinamide, formed through weak interactions between the API and a second organic molecule (*i.e.,* a coformer), were prepared and characterized with respect to their crystal form. Since pyrazinamide has an inherently good aqueous solubility and permeability at physiological pH, it was not expected to gain a significant improvement in either parameter from a classical enabling strategy like co-crystallisation. Thus, in the present work, we wished to use the established MCPA for simultaneous dissolution and permeation testing by investigating the effect of the aforementioned adducts on pyrazinamide performance.

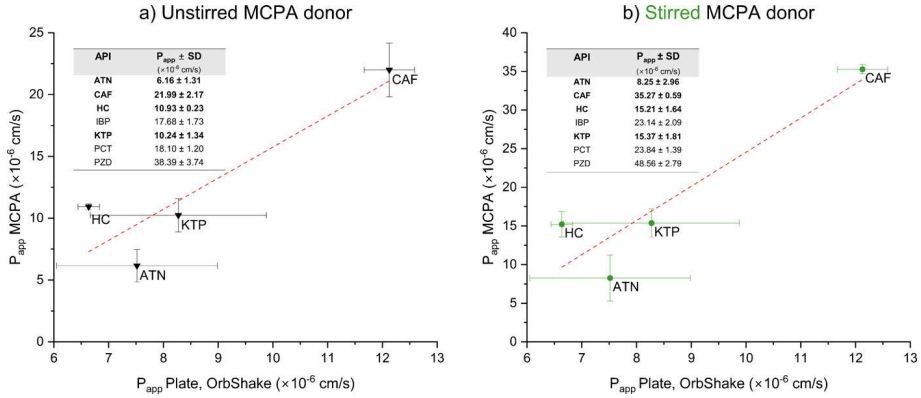

Figure 4. Correlation between the apparent permeability coefficients (P_{app}) of atenolol (ATN), caffeine (CAF), hydrocortisone (HC) and ketoprofen (KTP) measured with PermeaPad® plate in orbital shaker and in MCPA in unstirred (a; black triangles) and stirred (b; green circles) conditions. Red stippled lines intend to guide the eye and show the best-fit linear correlation between the two P_{app} values. Error bars show SD (n = 3). Inset tables show P_{app} ± SD values for all APIs tested with the MCPA, including ibuprofen (IBP), paracetamol (PCT) and pyrazinamide (PZD).

Table 3
In vitro fraction of dose absorbed after 3h (%F_a*) in MCPA (stirred conditions) for pyrazinamide (PZD) solutions, pure API and various crystalline adducts, as well as their molecular weights (M_w) and thermodynamic solubility (C_s). Results presented in order of increasing M_w as average ± SD.

Sample	Type	M_w (g/mol)	C_s (mM)	%F_a* (%)
unstirred solution	solution	123.113	100.72	8.27 ± 0.69
stirred solution				10.08 ± 1.86
PZD	pure drug suspension			10.23 ± 1.94
PZD-MLEA	salt suspension	239.213	220.41	10.67 ± 0.83
PZD-MLIA	co-crystal suspension	257.200	148.71	10.10 ± 0.85
PZD-MANDA		275.260	174.32	6.93 ± 0.49
PZD-DPA		290.233	64.61	7.75 ± 0.62
PZD-DHTA		321.243	25.68	8.16 ± 0.93
PZD-TRMA		333.253	24.58	8.19 ± 1.66

The probability of pyrazinamide to establish supramolecular interactions with different functional groups was studied with Mercury software (CCDC, Cambridge, UK). Atoms N7 and N4 (see Table 1) tend to interact preferentially with hydrogen bond donor groups, such as —OH or —COOH; a high probability of forming supramolecular synthons is also related to the amide group, which may act as both a hydrogen bond donor as well as an acceptor through the —NH and C=O groups, respectively. Based on this structural analysis and the pyrazinamide tendency to form supramolecular synthons, six carboxylic acids were selected as coformers for the co-crystallization: dihydroxyterephthalic acid (DHTA), maleic acid (MLEA), malic acid (MLIA), mandelic acid (MANDA), dipicolinic acid (DPA) and trimesic acid (TRMA). Further, the probability of an API forming a salt or a co-crystal with a coformer can be assessed *a priori* with high success rates through the empirical rule of ΔpK_a (ΔpKa = pK_a (protonated base) – pK_a [(acid)])[38] or related models.[27] According to this rule, $\Delta pK_a < -1$ yields exclusively non-ionized acid-base complexes, *i.e.* co-crystals, whilst the range -1—4 is viewed as uncertain and either an ionized salt or a co-crystal can be formed.[27] Following the ΔpK_a rule for all pyrazinamide—coformer pairs investigated in this work, these were predicted yield a co-crystal (Table 2).

The adduct formation was confirmed by a qualitative analysis employing FTIR-ATR spectroscopy and PXRD. These two techniques are able to discriminate between adducts and physical mixtures in a highly precise way, with a new and unique pattern from PXRD showing that a new crystal has been formed. FTIR was used to determine if the new crystals were adducts between pyrazinamide and the conformers. A shift in the peak corresponding to the acid functional group of the conformers would indicate that adducts had been formed. By evaluating the magnitude of this shift, it was possible to distinguish between crystalline salts and co-crystals.[39] The FTIR-ATR spectra (Appendix B, Fig. A2) of all crystalline adducts show consistent shifts of signals associated with both pyrazinamide and the respective coformers, proving the formation of the six new crystalline phases that differ from simple heterogeneous mixtures of the starting materials. Five crystalline adducts (PZD-DHTA, PZD-DPA, PZD-MANDA PZD-MLIA and PZD-TRMA) were determined to be cocrystals Interestingly, one of them, PZD-MLEA, having a ΔpK_a value closest to the uncertainty range of -1 to 4, albeit slightly under it (-1.32) was shown to be a molecular salt (see Appendix B, Fig. A2). This confirms the need for an experimental assessment of the ionic or neutral nature of newly formed crystalline adducts.[40,41] Moreover, from the diffraction patterns (Fig. S3) of the six adducts, it can be observed that all adducts show high crystallinity. It should be noted that in PZD-MANDA and PZD-TRMA, traces of unreacted coformer (below about 1—2 % w/w) were also present.

The adducts of smaller molecular weight (PZD-MLEA, PZD-MLIA and PZD-MANDA) showed higher thermodynamic solubility than the pure drug, whilst the larger ones (PZD-DPA, PZD-DHTA and PZD-TRMA) had lower solubility (Table 3). We chose, therefore, to focus on a scenario where all samples were far from their solubility limit and allow the dissolution rate of each crystal to dictate the permeation process.

The assumption made in this investigation is that the permeability of all co-formers can be considered negligible since, at neutral pH, all these compounds are in their ionic form and therefore permeability is regarded minimal.

Calculating P_{app} for a drug tested in a dissolution/permeation setup is not possible, since the donor concentration and, consequently, the concentration gradient driving the flux is changing throughout the course of the experiment. Thus, we chose to define the *in vitro* fraction of dose absorbed (%F_a*, Eq. (3)) over 3 hours (Q_{3h}), *i.e.*, the total amount of API accumulated into the fluidic acceptor media (Q_{tot}) normalized over the administered dose of the donor compartment (Q_0, Table 3).

$$\%F_a^* = \frac{Q_{tot}}{Q_0} * 100 \quad (3)$$

Interestingly, the same smaller adduct species (PZD-MLEA and PZD-MLIA) which expresses a higher solubility than pyrazinamide thermodynamic solubility permeated to the same or at least comparable degree as pyrazinamide solution (stirred). On the contrary, the permeation from the pyrazinamide unstirred solution was lower and more comparable to that of pyrazinamide from the larger crystalline adducts. Apart from the very general aforementioned trend, no significant differences between the crystal forms were observed (two-tailed Student's *t*-test at α = 0.05). Quite interestingly, PZD-MANDA showed a significantly lower %Fa* in comparison to all other formulations tested. Diffusion study performed on the PZD-MANDA solution showed an average diffusion coefficient of 8.53*10-6 cm^2/s, which is 7% lower than the diffusivity constant for pyrazinamide from a PBS solution (Table 1). As the diffusivity of a compound/adduct in UWL is controlled mostly by the hydrodynamic radii, these findings suggest the survival of a small population of the salt PDZ-MPLEA complex in solution, which reduces the net accumulation of pyrazinamide in the acceptor compartment. (Table 3). From a formulation screening respective, none of the investigated pyrazinamide formulation results superior to the pure drug suspension in terms of *in vitro* fraction dose absorbed (Table 3).

Hydrocortisone Amorphous Solid Dispersions

When designing ASDs, choosing the correct excipients (*e.g.*, polymers) can not only promote formulation stability but also allows the fine-tuning of the dissolution rate to best suit the formulation's purpose.[42] It should be underlined that altered or improved *in vitro* dissolution profile does not always translate into improved bioavailability.[25] Thus, it was of interest to explore the possibility of performing combined dissolution/permeation testing on ASDs in the MCPA. To this end, we prepared ASDs with either HPMC or PVP, yielding formulations with expectantly different release and permeation profiles owing to the polymers' properties (molecular weight and

lipophilicity). This concept of varying drug release profiles with PVP and HPMC has already been demonstrated for lyophilisates containing the same polymers in a recent work by Nielsen et al. for poorly soluble etoposide.[43]

The validity of the findings is supported by numerous studies, *e.g., in vivo* data for analogous BCS class II compound enzalutamide,[44] whose oral bioavailability from ASDs comprised of similar polymers was demonstrated to increase, in line with *in vitro* data.

Unlike pyrazinamide, hydrocortisone is a BCS class II drug, which exhibits low dissolution rate and relatively high permeability, making it a great candidate for enabling formulations that improve the solubility and/or dissolution rate of the drug. One such platform are ASDs, which have been shown to improve the permeability and bioavailability of drugs,[26] including hydrocortisone.[45] The greatest asset of these simple to prepare formulations is their ability to create and maintain a supersaturated state, *i.e.*, where the API is dissolved at a level above its thermodynamic solubility. This phenomenon is molecule-specific but fortunately, hydrocortisone has been shown to be capable of reaching supersaturation states.[46] Furthermore, hydrocortisone has been shown to maintain its supersaturated state when formulates as an ASD with HPMC[47] and studies have demonstrated the enhanced permeability of hydrocortisone from PVP-HC co-precipitates.[48]

The thermodynamic solubility (0.8 mM) of the crystalline drug was determined in a preliminary study to ensure enough of the ASD was used in the permeability testing to allow the formation of a supersaturated solution. Additionally, the successful amorphization of hydrocortisone by lyophilization was confirmed by DSC prior to the permeability experiments (thermogram shown in Appendix C, Fig. A4).

The results clearly demonstrate the advantage of both prepared ASDs, with HPMC being even better at promoting hydrocortisone permeation than PVP (Fig. 5). From the crystalline drug, in the course of 3 hours only 0.6 ± 0.1 % permeate the PermeaPad® membrane, while as much as double of the hydrocortisone from the PVP ASD reached the acceptor compartment (1.2 ± 0.2 %). For HPMC, the variation between replicates was quite high, as illustrated by the error bars in Fig. 5, but its superiority is nevertheless clear, as on average 2.1 ± 0.3 % of the initial amount of hydrocortisone has permeated by the end of the experiment. The variability in the HPMC-HC system could be explained by the nature of the lyophilizate, which was more porous than the PVP-HC one. This meant that the final ground powder of HPMC-HC had larger particle size and polydispersity than PVP-HC. This porosity could also contribute to faster dissolution rate and explain the differences in permeation behavior observed between the formulations. Another factor affecting the dissolution rate and consequently the flux of hydrocortisone is the smaller molecular weight and relative hydrophilicity of HPMC, compared to PVP, both factors causing more rapid expulsion of the drug and consequently higher solubilization. *In vivo* data for other BCS class II drugs has shown that ASDs-promoted quicker dissolution and higher supersaturation causing increased bioavailability.[49]

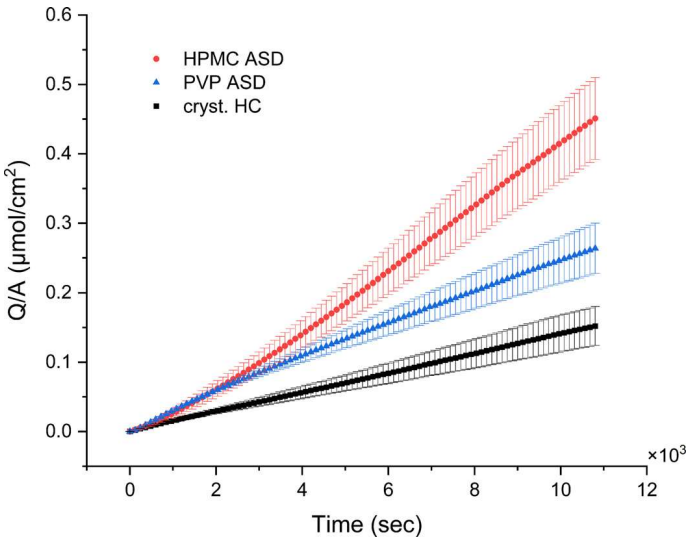

Figure 5. Permeation profiles of crystalline hydrocortisone (HC; black squares), and amorphous solid dispersions (ASDs) of the drug with hydrophilic polymers (hydroxypropyl)methyl cellulose (HPMC; red circles) and polyvinylpyrrolidone (PVP; blue triangles). Error bars show SD (n = 3).

These results suggest that both investigated formulations might offer a benefit to the bioavailability of hydrocortisone, although PVP might be better suited for a more sustained/prolonged drug release.

Conclusions

We have successfully developed and utilized a novel system for *in vitro* permeability testing suited for solid dosage form formulation testing. The system proved to be easy to set up and useful for discriminating between chemically diverse compounds in a predictive manner, and could be used for evaluating new drug candidates, as well as being used for early state formulation screening. Unlike other setups, with the MCPA is possible to have adjustable agitation in both the acceptor (*i.e.*, pumping driven fluid flow) and the donor (*i.e.*, magnetic stirring) compartments. This eliminates UWLs, thus facilitating an in-depth investigation of formulation under more physiologically relevant conditions. Overall, the system is user-friendly, cost-effective, and extremely adaptable with respect to volumes, flow/stirring speed, arrangement, and complexity. The experiments reported here were performed at room temperature, but, due to the limited size of the MIVO®s, it might be possible to place the diffusion cells inside an incubator and use different temperatures. With respect to the quantification method used, connecting the system to a spectrophotometer is a great improvement to the standard sampling protocol. However, manual sampling remains possible in case of very poorly soluble/permeable compounds with limited UV-detectability. Further development should include biorelevant media and lipolysis agent in the donor reactor and mucus on top of the PermeaPad®. This will convey the MCPA into an actual GI-on-a-chip. In conclusion, the obtained results show that MCPA's potential as a promising tool for a sustainable, easy implementable, cost-effective method for *in vitro* evaluation of drug performance.

Data availability

Data will be made available on request.

Declaration of Competing Interest

The authors declare the following financial interests/personal relationships which may be considered as potential competing interests: Associate Professor Massimiliano Pio Di Cagno, leading author of this paper, is the inventor of the PermeaPad® barrier and scientific consultant (5% position) for Phabioc GmbH, the manufacturer of PermeaPad®.

Dr. Silvia Scaglione is the founder of React4life S.p.A., the manufacturer of MIVO®.

Acknowledgements

The authors are grateful to Phabioc GmbH for supplying some of the PermeaPad® products used in this work. We would also like to

thank head engineer at UIO-SiteDel research group, Tove Larsen, for the technical support.

Supplementary materials

Supplementary material associated with this article can be found in the online version at doi:10.1016/j.xphs.2023.12.012.

References

1. Fedi A, Vitale C, Ponschin G, Ayehunie S, Fato M, Scaglione S. In vitro models replicating the human intestinal epithelium for absorption and metabolism studies: a systematic review. *J Control Release*. 2021;335:247–268. https://10.1016/j.jconrel.2021.05.028.
2. O'Shea JP, Augustijns P, Brandl M, Brayden DJ, Brouwers J, Griffin BT, Holm R, Jacobsen A-C, Lennernäs H, Vinarov Z, O'Driscoll CM. Best practices in current models mimicking drug permeability in the gastrointestinal tract - an UNGAP review. *Eur J Pharm Sci*. 2022;170.106098-106098; https://10.1016/j.ejps.2021.106098.
3. Nunes R, Silva C, Chaves L. 4.2 - Tissue-based in vitro and ex vivo models for intestinal permeability studies. Ed. In: Sarmento B, ed. *Concepts and Models for Drug Permeability Studies*. Woodhead Publishing; 2016:203–236.
4. Pereira C, Costa J, Sarmento B, Araújo F. 3.3 - Cell-based in vitro models for intestinal permeability studies. Ed. In: Sarmento B, ed. *Concepts and Models for Drug Permeability Studies*. Woodhead Publishing; 2016:57–81.
5. Berben P, Bauer-Brandl A, Brandl M, Faller B, Flaten GE, Jacobsen A-C, Brouwers J, Augustijns P. Drug permeability profiling using cell-free permeation tools: overview and applications. *Eur J Pharm Sci*. 2018;119:219–233. https://10.1016/j.ejps.2018.04.016.
6. Jacobsen A-C, Visentin S, Butnarasu C, Stein PC, di Cagno MP. Commercially available cell-free permeability tests for industrial drug development: increased sustainability through reduction of in vivo studies. *Pharmaceutics*. 2023;15(2):592. https://10.3390/pharmaceutics15020592.
7. Bibi HA, di Cagno M, Holm R, Bauer-Brandl A. Permeapad™ for investigation of passive drug permeability: the effect of surfactants, co-solvents and simulated intestinal fluids (FaSSIF and FeSSIF). *Int J Pharm*. 2015;493(1-2):192–197. https://10.1016/j.ijpharm.2015.07.028.
8. Pion1. BioFLUXTM, 2020. Retrieved from: https://pion-inc.com/scientific-instruments/in-vivo-predictive-tools/absorption/bioflux.
9. Pion2. MacroFLUXTM, 2020. Retrieved from: https://pion-inc.com/analytical-services/formulation/dissolution-absorption/macroflux.
10. Sironi D, Rosenberg J, Bauer-Brandl A, Brandl M. PermeaLoop™, a novel in vitro tool for small-scale drug-dissolution/permeation studies. *J Pharm Biomed Anal*. 2018;156:247–251. https://10.1016/j.jpba.2018.04.042.
11. Eriksen JB, Messerschmid R, Andersen ML, Wada K, Bauer-Brandl A, Brandl M. Dissolution/permeation with PermeaLoop™: experience and IVIVC exemplified by dipyridamole enabling formulations. *Eur J Pharm Sci*. 2020;154. 105532-105532; https://10.1016/j.ejps.2020.105532.
12. Holzem FL, Weck A, Schaffland JP, Stillhart C, Klein S, Bauer-Brandl A, Brandl M. Biopredictive capability assessment of two dissolution/permeation assays, μFLUX™ and PermeaLoop™, using supersaturating formulations of Posaconazole. *Eur J Pharm Sci*. 2022;176. 106260-106260; https://10.1016/j.ejps.2022.106260.
13. Nunes PD, Pinto JF, Bauer-Brandl A, Brandl M, Henriques J, Paiva AM. In vitro dissolution/permeation tools for amorphous solid dispersions bioavailability forecasting I: experimental design for PermeaLoop. *Eur J Pharm Sci*. 2023;188: 106512. https://10.1016/j.ejps.2023.106512.
14. Marrella A, Buratti P, Markus J, Firpo G, Pesenti M, Landry T, Ayehunie S, Scaglione S, Kandarova H, Aiello M. In vitro demonstration of intestinal absorption mechanisms of different sugars using 3d organotypic tissues in a fluidic device. *ALTEX*. 2020;37(2):255–264. https://10.14573/altex.1908311.
15. Marzagalli M, Pelizzoni G, Fedi A, Vitale C, Fontana F, Bruno S, Poggi A, Dondero A, Aiello M, Castriconi R, Bottino C, Scaglione S. A multi-organ-on-chip to recapitulate the infiltration and the cytotoxic activity of circulating NK cells in 3D matrix-based tumor model. *Front Bioeng Biotechnol*. 2022;10. 945149-945149; https://10.3389/fbioe.2022.945149.
16. Pulsoni I, Lubda M, Aiello M, Fedi A, Marzagalli M, von Hagen J, Scaglione S. Comparison between franz diffusion cell and a novel micro-physiological system for in vitro penetration assay using different skin models. *SLAS Technol*. 2022;27(3):161–171. https://10.1016/j.slast.2021.12.006.
17. di Cagno MP, Bibi HA, Bauer-Brandl A. New biomimetic barrier Permeapad™ for efficient investigation of passive permeability of drugs. *Eur J Pharm Sci*. 2015;73:29–34. https://10.1016/j.ejps.2015.03.019.
18. WHO. (2009). Biopharmaceutics Classification System (BCS)-based biowaiver applications: anti-tuberculosis medicines. Guidance document. FDA: WHO prequalification of medicines programme.
19. Shan N, Zaworotko MJ. The role of cocrystals in pharmaceutical science. *Drug Discov Today*. 2008;13(9):440–446. https://10.1016/j.drudis.2008.03.004.
20. Abourahma H, Cocuzza DS, Melendez J, Urban JM. Pyrazinamide cocrystals and the search for polymorphs. *Cryst Eng Comm*. 2011;13(21):6442–6450. https://10.1039/c1ce05598d.
21. Bordignon S, Cerreia Vioglio P, Priola E, Voinovich D, Gobetto R, Nishiyama Y, Chierotti MR. Engineering codrug solid forms: mechanochemical synthesis of an indomethacin–caffeine system. *Cryst Growth Des*. 2017;17(11):5744–5752. https://10.1021/acs.cgd.7b00748.
22. Bordignon S, Vioglio PC, Amadio E, Rossi F, Priola E, Voinovich D, Gobetto R, Chierotti MR. Molecular crystal forms of antitubercular ethionamide with dicarboxylic acids: solid-state properties and a combined structural and spectroscopic study. *Pharmaceutics*. 2020;12(9):1–18. https://10.3390/pharmaceutics12090818.
23. Latif S, Abbas N, Hussain A, Arshad MS, Bukhari NI, Afzal H, Riffat S, Ahmad Z. Development of paracetamol-caffeine co-crystals to improve compressional, formulation and in vivo performance. *Drug Dev Ind Pharm*. 2018;44(7):1099–1108. https://10.1080/03639045.2018.1435687.
24. Pandey N, Ghosh A. An outlook on permeability escalation through cocrystallization for developing pharmaceuticals with improved biopharmaceutical properties. *J Drug Deliv Sci Technol*. 2022;76: 103757. https://10.1016/j.jddst.2022.103757.
25. Liu J, Grohganz H, Lobmann K, Rades T, Hempel N-J. Co-amorphous drug formulations in numbers: recent advances in co-amorphous drug formulations with focus on co-formability, molar ratio, preparation methods, physical stability, in vitro and in vivo performance, and new formulation strategies. *Pharmaceutics*. 2021;13(3):389. https://10.3390/pharmaceutics13030389.
26. Schittny A, Huwyler J, Puchkov M. Mechanisms of increased bioavailability through amorphous solid dispersions: a review. *Drug Deliv*. 2020;27(1):110–127. https://10.1080/10717544.2019.1704940.
27. Cruz-Cabeza AJ. Acid-base crystalline complexes and the pKa rule. *Cryst Eng Comm*. 2012;14(2):6362–6365. https://10.1039/c2ce26055g.
28. Jacobsen A-C, Krupa A, Brandl M, Bauer-Brandl A. High-throughput dissolution/permeation screening—a 96-well two-compartment microplate approach. *Pharmaceutics*. 2019;11(5):227. https://10.3390/pharmaceutics11050227.
29. Tzanova MM, Randelov E, Stein PC, Hiorth M, Di Cagno MP. Towards a better mechanistic comprehension of drug permeation and absorption: introducing the diffusion-partitioning interplay. *Int J Pharm*. 2021;608:9. https://10.1016/j.ijpharm.2021.121116.
30. Chen J, Brooks CL, Scheraga HA. Revisiting the carboxylic acid dimers in aqueous solution: interplay of hydrogen bonding, hydrophobic interactions, and entropy. *J Phys Chem B*. 2008;112(2):242–249. https://10.1021/jp074355h.
31. Demkin AG, Kolesov BA. Tautomeric hydrogen bond in dimers of ibuprofen. *J Phys Chem A*. 2019;123(26):5537–5541. https://10.1021/acs.jpca.9b02813.
32. Yang Y, Faustino PJ, Volpe DA, Ellison CD, Lyon RC, Yu LX. Biopharmaceutics classification of selected β-blockers: solubility and permeability class membership. *Mol Pharmaceutics*. 2007;4(4):608–614. https://10.1021/mp070028i.
33. Eriksen JB, Jacobsen A-C, Christensen KT, Bauer-Brandl A, Brandl M. 'Stirred not Shaken!' comparing agitation methods for permeability studies using a novel type of 96-well sandwich-plates. *J Pharm Sci*. 2022;111(1):32–40. https://doi.org/10.1016/j.xphs.2021.06.006.
34. Yazdanian M, Glynn SL, Wright JL, Hawi A. Correlating partitioning and caco-2 cell permeability of structurally diverse small molecular weight compounds. *Pharm Res*. 1998;15(9):1490–1494. https://10.1023/A. 1011930411574.
35. Jacobsen A-C, Nielsen S, Brandl M, Bauer-Brandl A. Drug permeability profiling using the novel Permeapad® 96-well plate. *Pharm Res*. 2020;37(6):93. https://10.1007/s11095-020-02807-x.
36. Teksin ZS, Seo PR, Polli JE. Comparison of drug permeabilities and BCS classification: three lipid-component PAMPA system method versus Caco-2 monolayers. *AAPS J*. 2010;12(2):238–241. https://10.1208/s12248. 010-9176-2.
37. Zhu C, Jiang L, Chen T-M, Hwang K-K. A comparative study of artificial membrane permeability assay for high throughput profiling of drug absorption potential. *Eur J Med Chem*. 2002;37(5):399–407. https://10.1016/S0223-5234(02). 01360-0.
38. Bhogala BR, Basavoju S, Nangia A. Tape and layer structures in cocrystals of some di- and tricarboxylic acids with 4,4′-bipyridines and isonicotinamide. From binary to ternary cocrystals. *Cryst Eng Comm*. 2005;7(90):551–562. https://10.1039/b509162d.
39. Birolo R, Bravetti F, Bordignon S, D'Abbrunzo I, Mazzeo PP, Perissutti B, Bacchi A, Chierotti MR, Gobetto R. Overcoming the Drawbacks of sulpiride by means of new crystal forms. *Pharmaceutics*. 2022;14(9):1754. https://10.3390/pharmaceutics14091754.
40. Aramini A, Bianchini G, Lillini S, Bordignon S, Tomassetti M, Novelli R, Mattioli S, Lvova L, Paolesse R, Chierotti MR, Allegretti M. Unexpected salt/cocrystal polymorphism of the ketoprofen–lysine system: discovery of a new ketoprofen–l-lysine salt polymorph with different physicochemical and pharmacokinetic properties. *Pharmaceuticals*. 2021;14(6):555. https://10.3390/ph14060555.
41. Bernasconi D, Bordignon S, Rossi F, Priola E, Nervi C, Gobetto R, Voinovich D, Hasa D, Duong NT, Nishiyama Y, Chierotti MR. Selective synthesis of a salt and a cocrystal of the ethionamide–salicylic acid system. *Cryst Growth Des*. 2020;20(2):906–915. https://10.1021/acs.cgd.9b01299.
42. Dengale SJ, Grohganz H, Rades T, Löbmann K. Recent advances in co-amorphous drug formulations. *Adv Drug Deliv Rev*. 2016;100:116–125. https://10.1016/j.addr.2015.12.009.
43. Nielsen RB, Larsen BS, Holm R, Pijpers I, Snoeys J, Nielsen UG, Tho I, Nielsen CU. Increased bioavailability of a P-gp substrate: Co-release of etoposide and zosuquidar from amorphous solid dispersions. *Int J Pharm*. 2023;642:123094-123094; https://10.1016/j.ijpharm.2023.123094.
44. Wilson VR, Lou X, Osterling DJ, Stolarik DF, Jenkins GJ, Nichols BLB, Dong Y, Edgar KJ, Zhang GGZ, Taylor LS. Amorphous solid dispersions of enzalutamide and novel polysaccharide derivatives: investigation of relationships between polymer structure and performance. *Sci Rep*. 2020;10(1):18535. https://10.1038/s41598-020-75077-7.
45. Altamimi MA, Elzayat EM, Qamar W, Alshehri SM, Sherif AY, Haq N, Shakeel F. Evaluation of the bioavailability of hydrocortisone when prepared as solid

dispersion. *Saudi Pharm J*. 2019;27(5):629–636. https://10.1016/j.jsps.2019.03.004.

46. Davis AF, Hadgraft J. Effect of supersaturation on membrane transport: 1. Hydrocortisone acetate. *Int J Pharm*. 1991;76(1):1–8. https://10.1016/0378-5173(91).90337-N.
47. Yang X, Shen B, Huang Y. Mechanistic study of HPMC-prolonged supersaturation of hydrocortisone. *Cryst Growth Des*. 2015;15(2):546–551. https://10.1021/cg501784n.
48. Corrigan OI, Farvar MA, Higuchi WI. Drug membrane transport enhancement using high energy drug polyvinylpyrrolidone (PVP) co-precipitates. *Int J Pharm*. 1980;5(3):229–238. https://10.1016/0378-5173(80)90130-1.
49. Adeli E. Irbesartan-loaded electrospun nanofibers-based PVP K90 for the drug dissolution improvement: fabrication, in vitro performance assessment, and in vivo evaluation. *J Appl Polym Sci*. 2015;132(27). p. np-n/a; https://10.1002/app.42212.